Materials Letters 63 (2009) 1159–1161

Contents lists available at ScienceDirect

Materials Letters

journal homepage: www.elsevier.com/locate/matlet

Thermo-XRD and differential scanning calorimetry to trace epitaxial crystallization in PA6/montmorillonite nanocomposites

Africa Yebra-Rodríguez [a,*], Pedro Alvarez-Lloret [b], Alejandro B. Rodríguez-Navarro [b], Jose Daniel Martín-Ramos [b], Carolina Cardell [b]

[a] Department of Geology, Faculty of Experimental Science, University of Jaén, Campus Las Lagunillas s/n, 23071 Jaén, Spain
[b] Department of Mineralogy and Petrology, Faculty of Science, University of Granada, Campus Fuentenueva s/n, 18071 Granada, Spain

ARTICLE INFO

Article history:
Received 7 October 2008
Accepted 11 February 2009
Available online 21 February 2009

Keywords:
Nanocomposite
Montmorillonite
Thermo-XRD
DSC
Epitaxial crystallization

ABSTRACT

The physical properties of montmorillonite–polyamide nanocomposites, which in turn determine varied industrial applications are greatly dependent on polymer crystal structure and crystallinity. Thus, control of polyamide crystallization is critical, especially when this polymer adopts different polymorphic structures. To fully characterize the crystallization behavior of this nanocomposite by increasing temperature, this work presents for the first time an innovative approach based on combined new thermo-X-ray diffraction (TXRD) routines for 2D mapping and differential scanning calorimetry (DSC) techniques. Results reveal that: (i) organically modified montmorillonite included in the polymer matrix, composed of polyamide-6, increases the thermal stability of the nanocomposite, and (ii) epitaxial mechanisms explain the nucleation of the thermodynamically less stable γ crystal phase reported in the literature.

© 2009 Elsevier B.V. All rights reserved.

1. Introduction

Nanocomposite material structures composed of clay nanolayers (typically montmorillonite) in a polymeric matrix exhibit remarkable physical properties suitable for sophisticated industrial applications [1–5]. It is recognized that thermal and mechanical properties of both pristine polymers and polymer–clay nanocomposites are greatly influenced by crystal properties [6–8]. Polyamide-6 (PA6) crystallizes in three possible structure types: α, β and γ. The stable monoclinic α structure organizes in planar zig-zag chains (H-bonded sheets), whereas the metastable, pseudo-hexagonal γ structure is organized in a twisted chain (not collinear and with longer H-bond lengths) [9]. The less well-known mesomorphic β structure is considered an intermediate state between the former two [10].

To fully understand the thermal properties of such nanocomposites, this paper investigates the crystal modifications in PA6 crystals prompted by increasing temperature (*T*) up to 230 °C. Moreover, another major goal of this research is to evaluate the benefits of combined new TXRD routines for 2D mapping and DSC to investigate the crystallization mechanism of PA6 and montmorillonite-reinforced PA6 nanocomposites (PA6/MMT) due to *T* transitions. TXRD is a suitable and powerful technique to study *T*-induced phase transitions and crystalline processes in many research fields connected to material sciences, chemistry, metallurgy and cultural heritage science, among others [11–13]. Recently, TXRD has been proven to be an especially effective tool to better recognize the evolution of physicochemical processes susceptible to monitoring by XRD thanks to the use of innovative 2D mapping routines implemented with the *XPowder PLUS* software [14]. Our work presents for the first time 2D TXRD maps for nanocomposites thus allowing a better interpretation of *T*-induced nanocomposite changes in structure types.

2. Experimental

This investigation was conducted on injection-molded samples of PA6 and PA6/MMT. Both samples were manufactured with commercial PA6 (Ultramid®) and 5 wt.% montmorillonite modified with methyl tallow bis-2-hydroxyethyl quaternary ammonium chloride (Southern Clay Products, Inc.). The nanocomposites were manufactured as described elsewhere [8] and injected to simulate industrial processes.

In situ XRD data were acquired using a Philips PW1710/00 X-ray diffractometer with PW1712 communication card via RS232 serial port, full-duplex controlled by the *XPowder PLUS* software [14]. The heating device is composed of an halogen lamp (Philips Capsule-line Pro 75 W, 12 V) that heats the XRD chamber up to 230 °C, a Pt-1000 probe for *T* monitoring (0.5 °C precision), and a software-controlled thermostat with digital *T* selection. A detailed description of the heating system is described elsewhere [13]. The XRD patterns were scanned over $15<°2\theta<30$ range, with 0.1 goniometric rate and 0.4 s integration time. Backgrounds of diffraction patterns were subtracted. The scan mode was continuous using CuKα radiation. The voltage was 40 kV, and the tube current 40 mA. Diffraction patterns were collected at 10 °C increments between 30 and 230 °C. Phase transformation was

* Corresponding author. Tel.: +34 953212945; fax: +34 953212946.
E-mail address: ayebra@ujaen.es (A. Yebra-Rodríguez).

0167-577X/$ – see front matter © 2009 Elsevier B.V. All rights reserved.
doi:10.1016/j.matlet.2009.02.027

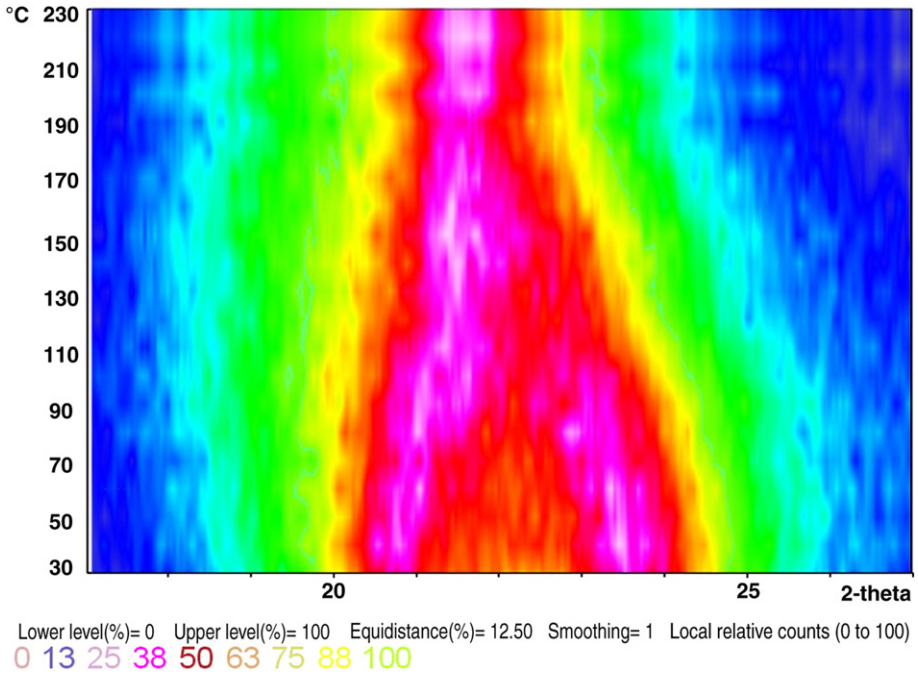

Fig. 1. 2D TXRD map for PA6 sample. Note that the main PA6 α diffraction peaks (~20.2 and 24 °2θ) diminish while PA6 γ diffraction peak (~21.3 °2θ) gradually appears up to 170 °C.

simply detected by the appearance/disappearance of characteristic peaks in the XRD patterns. Thermal analysis performed with DSC (DSC 822e/700 Mettler Toledo) was applied on samples after drying by vacuum heating at 80 °C during 48 h (heating rate: 20 °C/min over a *T* range of 25–270 °C).

3. Results and discussion

The TXRD results for PA6 shown as 2D mapping in Fig. 1 indicate that the thermodynamically more stable α structure is prominent. The distinctive diffraction lines of α structure appear at ~20.2 (200) and 24 (201/202) °2θ, and the strongest diffraction line for the γ structure is seen at ~21.3 (100) °2θ. The TXRD map (Fig. 1) shows the onset of the phase transition from α toward γ structure occurs at ~90 °C. One of the benefits of applying this novel 2D TXRD mapping routine is straightforward imaging of the α–γ phase conversion, a non-isothermal transformation (between ~90 and 150 °C) that takes place as a solid-state reaction (Brill Transition type) with no amorphous-mediated step, as indicated by the absence of background noise (no narrow horizontal bands) throughout the conversion. Above 170 °C the γ structure is the only crystal phase present, since the lack of horizontal bands suggest that no amorphization process takes place before the melting *T* is achieved.

The occurrence of the γ structure in nylon-6 polymers at high temperature (250 °C) has been already reported [15]. The volume per chain is smaller for the γ structure, and consequently the cohesive energy density is slightly larger than in the α form. The calculated H–H

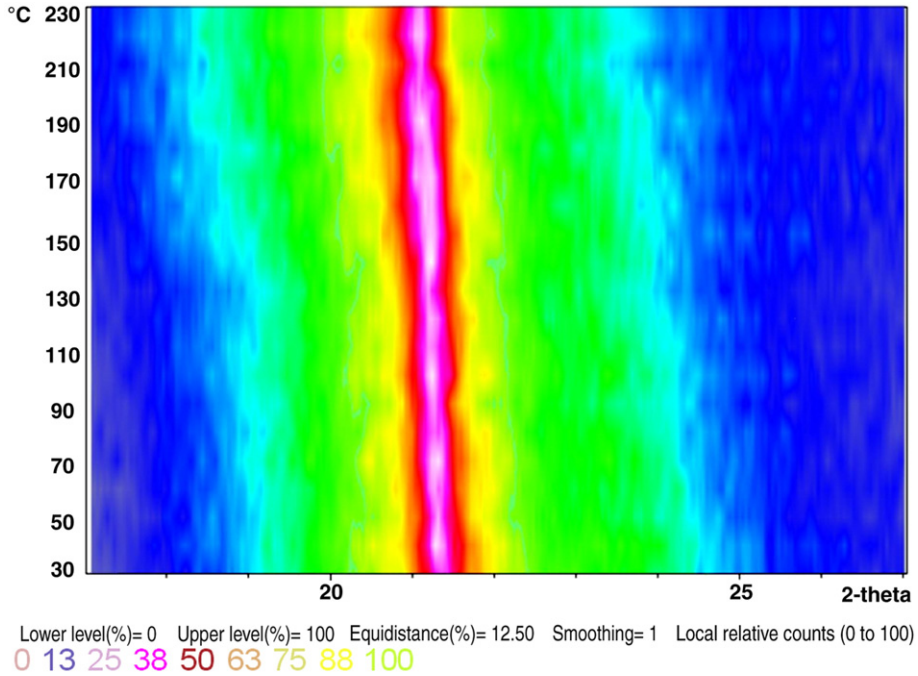

Fig. 2. 2D TXRD map for PA6/MMT sample. The XRD line of PA6/MMT appears at ~21.3 °2θ remaining unchanged during heating.

non-bonded distances in the α structure (2.140 Å) are significantly shorter than those in the γ structure (2.466 Å) [16]. Taking into account that the optimum packing of the methylene units occurs in polyethylene [17], the increased number of methylene groups makes the γ structure the most efficient in terms of packing, and therefore more stable than the α at high temperatures.

Fig. 2 shows the TXRD map for PA6/MMT where only the γ structure is exhibited. This indicates that the presence of montmorillonite in the polymer matrix increases thermal stability of nanocomposites since no phase transformation takes place that may induce undesirable effects, such as volumetric dilatation. Moreover, the 2D maps method revealed that the nanocomposite maintains its crystallinity with rising *T*, as indicated by the constant FWHM of the vertical band corresponding to the γ structure.

DSC analyses of the PA6 sample (Fig. 3) display a peak at ~223 °C, which corresponds to the melting *T* of the PA6 α structure. Nanocomposite sample shows a double melting peak at ~212 and 222 °C, the typical melting *T* for γ and α structures, respectively. In the XRD analysis, the scarce amount of α crystals in the PA6/MMT sample was masked by the stronger diffraction peak of the γ structure. The γ crystals grow preferentially near the surface of the montmorillonite layers, while the α crystals develop where the nanolayers do not influence chain conformation and folding of the PA6. The cause of this is that montmorillonite impedes the shifting of H-bonds associated with the transformation from γ to thermodynamically more stable α structures [8,18].

We have observed that the presence of montmorillonite favors nucleation of the thermodynamically less stable PA6 γ phase. Ionic mineral surfaces can facilitate the absorption of polymers by electrostatic interactions and could promote their nucleation and crystallization [19]. However, the latter mechanism does not explain the selection of a specific PA6 polymorphic phase as seen in this work. This behavior could be explained by stereochemical and geometrical matching mechanisms implying that the arrangement of the functional groups of the polymer matches or reproduces to some degree the disposition of ionic groups in the mineral surface [20,21]. Thus, polymer molecules could be deposited on the surface with an alignment partially induced by the orientation of ion rows in the mineral substrate [22] and partially induced by the shear flow during injection molding. The amide groups along the polymer chain form H bonds to rows of OH ions in the basal plane of the montmorillonite and become aligned along the *a*-axis crystallographic direction. In fact, there is good correspondence between the *a* lattice parameters of montmorillonite (5.2 Å) and the spacing between every two amide groups in the polyamide chain (5.0 Å). This type of epitaxial mechanism favors nucleation of the polymorphic phase of the polymer having a crystallographic structure most compatible with the montmorillonite surface [23,24].

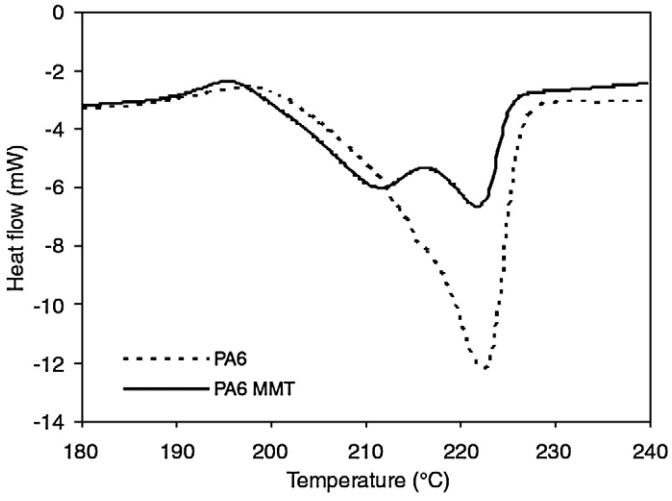

Fig. 3. DSC heating process of PA6 and PA6/MMT.

4. Conclusions

The new TXRD routines for 2D mapping offer new insight to better imaging and understanding the reaction trends and phase transformation kinetics occurring in nanocomposites below the melting *T*. Organic modified montmorillonite included in the polymer matrix, composed of PA6, increases the thermal stability of the nanocomposite. Epitaxial mechanisms explain the nucleation of the thermodynamically less stable γ crystal phase reported in the literature [25]. In the context of nanomaterials, the singular characteristics of nanocomposites – in terms of structure, chemistry, mechanics, dynamics and response – offer numerous experimental and conceptual research opportunities in emerging nanosciences.

Acknowledgement

This research was supported by Research Groups RNM-325 and RNM-179 (CICE, JA, Spain). We wish to thank Dr. Ana Jiménez (Servicios Técnicos de Investigación, University of Jaén, Spain) for DSC data collection and A. Kowalski for English revision.

References

[1] Kojima Y, Usuki A, Kawasumi M, Okada A, Fukushima Y, Kurauchi T, et al. J Mater Res 1993;8:1185–9.
[2] Wang S, Hu Y, Zonga R, Tanga Y, Chen Z, Fan W. Appl Clay Sci 2004;25:49–55.
[3] Aranda P, Darder M, Fernández-Saavedra R, López-Blanco M, Ruiz-Hitzky E. Thin Sol Films 2006;495:104–12.
[4] Ray S, Quek SY, Easteal A, Chen XD. Int J Food Eng 2006;2:1–11.
[5] Vora RH, Vora M. Mater Sci Eng 2006;B132:90–102.
[6] Kojima Y, Usuki A, Kawasumi M, Okada A, Kurauchi T, Kamigaito O, et al. J Polym Sci Part B: Polym Phys 1995;33:1039–45.
[7] Chen B, Evans JRG, Greenwell HC, Boulet P, Coveney PV, Bowdenf AA, et al. Chem Soc Rev 2008;37:568–94.
[8] Yebra-Rodríguez A, Alvarez-Lloret P, Cardell C, Rodríguez-Navarro A. Appl Clay Sci 2009;43:91–7.
[9] Arimoto H, Ishibashi M, Hirai M. J Polym Sci 1965;A3:317–26.
[10] Xenopoulos A, Clark ES. Physical structures. In: Kochan MI, editor. Nylon Plastics Handbook. Munich: Hanser Publishers; 1995. p. 108–37.
[11] Barre M, Le Berre F, Crosnier-Lopez MP, Bohnke O, Emery J, Fourquet JL. Chem Ater 2006;18:5486–91.
[12] Correcher V, Garcia-Guinea J, Valle-Fuentes FJ. J Therm Anal Calorim 2006;83:439–44.
[13] Cardell C, Sánchez-Navas A, Olmo-Reyes FJ, Martín-Ramos JD. Anal Chem 2007;79:4455–62.
[14] Martín-Ramos JD. Using XPowder: a software package for powder X-ray diffraction analysis. *http://www.xpowder.com* (accessed March 15, 2004).
[15] Lincoln DM, Vaia RA, Wang ZG, Hsiao BS. Polymer 2001;42:1621–31.
[16] Dasgupta S, Hammond WB, Goddard WA. J Am Chem Soc 1996;118:12291–301.
[17] Karasawa N, Dasgupta S, Goddard WA. J Phy Chem 1991;95:2260–72.
[18] Fornes TD, Paul DR. Polymer 2003;44:3945–61.
[19] Norde W, Lyklema JJ. Biomater Sci Polymer Edn 1991;2:183–202.
[20] Addadi L, Moradian J, Shay E, Maroudas NG, Weiner S. Proc Natl Acad Sci 1987;84:2732–6.
[21] Mann S. Nature 1988;332:119–24.
[22] Carr SH, Keller A, Baer E. J Polym Sci Part A-2: Phys 1970;8:1467–90.
[23] Lahav M, Leiserowitz L. J Phys 1993;D26:B22–31.
[24] Black SN, Bromley LA, Cottier D, Davey RJ, Dobbs B, Rout JE. J Chem Soc Faraday Trans 1991;87:3409–14.
[25] Giannelis EP. Adv Mater 1996;8:29–35.